Indian Journal of Pure & Applied Physics
Vol. 60, April 2022, pp. 325-334

Photocatalytic Degradation of Congo Red and Methyl Orange Dye Under Visible Light Using Silver and Iron co-doped TiO_2 Nanoparticles

Anju Rani[a], Suresh Kumar[a], R L Dhiman[b]*, Virender Singh[c] & Suresh Kumar[c]

[a]Department of Physics, M.M. (Deemed to be University), Mullana-Ambala, Haryana- 133 207 India
[b]Department of Physics, Sanatan Dharma College, Ambala Cantt. Haryana- 133 001 India
[c]Department of Electronic Science, Kurukshetra University, Kurukshetra, Haryana- 136 119 India

Received 27 December 2021; accepted 23 March 2022

In the present report TiO_2 nanoparticles co-doped with iron and different mol % of silver have been successfully synthesized by sol-gel route and studied by X-ray diffraction (XRD), Energy dispersive X-ray spectroscopy (EDX), UV-visible absorption spectroscopy (UV-Vis), Photoluminescence spectroscopy (PL), Field emission scanning electron microscopy (FESEM), Transmission electron microscopy (TEM), and FTIR spectroscopy. The XRD data analysis confirms the formation of mixed phases of TiO_2 (anatase) and Ag_2O phase. The crystalline size was vary from 48.0 nm to 44.6 nm determined from XRD further verified from TEM micrograph. The EDXS measurements suggest that iron is completely incorporated however silver has not incorporated into TiO_2 matrix. The optical band gap of the prepared nanoparticles was calculated by UV-Visible absorption spectroscopy using Tauc-Davis and Mott expression and found to varying from 2.92 to 2.30 eV. The absorption bands in the UV-visible spectra shift towards higher wave length region and appearance of emission bands in PL spectra confirms the formation of energy substates in the forbidden gap of the prepared samples. TEM micrographs showed that prepared nanoparticles are somewhat spherical in shape. The formation of different functional groups and bonds in the structure of synthesized nanoparticles as observed in FTIR spectra helps in degradation of organic dyes (congo red and methyl orange) and enhance the photocatalytic activity under visible light. It is observed that the higher doping concentration of silver causes to decrease the band gap energy as a result the carrier recombination rate decreases and therefore enhance the degradation efficiency.

Keywords: Co-doped TiO_2 nanoparticles; XRD; SEM; TEM; Photoluminescence; Photocatalysis

1 Introduction

Organic dyes are mainly used as coloring agents in cosmetics, leather, paper, textiles, food, plastics, and other industries. These dyes contain toxic synthetic colors and due to its complex structure and high stability are not easily biodegradable. Direct discharge of these dyes without any treatment can impact hazardous effects on human beings as well as on the environment[1-2]. Thus, decomposition of such organic dyes prior to discharge of wastewater from dye industries is significantly important. Out of various physico-chemical methods photocatalysis is gaining considerable interest in the field of removal of organic dyes from waste water due to its environment friendly technology and do not requires any further treatment for secondary disposal[3-6]. During last decades scientist have draw their more attention towards the development of highly effective TiO_2 semiconductor based photocatalyst for degradation of organic dyes dissolved in wastewater. In recent years co-doped TiO_2 semiconductor photocatalysts nanoparticles are most widely studied because of its low cost of production, high stability and high catalytic efficiency for degradation of organic dyes[7-9]. Several techniques have been employed by researchers to synthesize co-doped TiO_2 nanoparticles. Sol-gel is a most simple technique having high control on shape, size, structure and surface morphology[10]. The photocatalytic efficiency of co-doped TiO_2 nanoparticles is still limited due to following reasons one is the TiO_2 have large band gap (Eg=3.2 eV) which restricted its absorption to UV irradiation and second one is the fast recombination rate of photogenerated electron hole pairs[11-12]. Researchers are continuously doing work for the achievement of higher photocatalytic activity of doped TiO_2 nanomaterials under visible light. The transitional metal ions are widely doped to enhance photocatalytic activity of TiO_2 semiconductor[13]. The role of doped transition metal

*Corresponding author:
(E-mail: roshandhiman_kuk@yahoo.co.in)

ions in TiO_2 is allow to absorb more visible light range and trap more carriers leads to improve the photocatalytic activity. It has been reported that silver and iron co-doped TiO_2 nanoparticles exhibit an enhanced charge carrier separation and improve photocatalytic activity for degradation of organic dyes[14-15]. Single metal e.g. Ag/ Fe doped TiO_2 nanoparticles fabricated by sol-gel technique showed enhanced photocatalytic activity under visible light irradiation[16-17]. Fe-Pr co-doped nanoparticles synthesized by sol-gel technique and higher enhance in photocatalytic activity was observed under visible light[18]. Excellent performance for photocatalytic degradation of organic pollutants (MB dye) under visible light was observed using Co-Fe co-doped nanoparticles synthesized by solvothermal method[19]. It has been reported that doping of two different metals in TiO_2 semiconductor remarkable enhance the photocatalytic activity for degradation of organic pollutants in comparison to single metal doping[20-24]. Therefore we have planned to synthesized silver and iron co-doped TiO_2 nanoparticles by sol-gel method. The synthesized samples were characterized by XRD, EDX Spectroscopy, UV-Vis spectroscopy, Photoluminescence spectroscopy, FESEM, TEM, FTIR Spectroscopy in order to study the effect of co-doping on photocatalytic activity for the degradation of congo red and methyl orange dyes under visible light.

2 Experimental Details

2.1 Chemicals and reagents

All Analytical Regent grade materials e.g. Titanium (IV) isopropoxide ($Ti\{OCH(CH_3)_2\}_4$ supplied by Sigma-aldrich, Silver nitrate ($AgNO_3$) supplied by Merck and Ferric Chloride ($FeCl_3$) supplied by HIMEDIA were used as the Source of TiO_2 precursor , silver and iron respectively. The pH of the solution was maintained by a conc. HNO_3 and Methanol (CH_3OH). The Deionized water (DI) was used as solvent in whole synthesis process.

2.2 Synthesis of nanoparticles

The silver and iron co-doped TiO_2 nanoparticles were synthesized via sol gel route by adopting the following procedure. 13 ml of Titanium (IV) isoproxide (TTIP) was hydrolyses with 50 ml of methanol and 0.3gm of $AgNO_3$ was dissolved in DI water separately. To maintained pH valve (2-3) of the dissolved solution 0.8 ml of concentrated HNO_3 was added drop by drop in TTIP solution and the dissolved solution was stirred for 1 h. In very small amount of DI water 0.4 gm Ferric Chloride ($FeCl_3$) was dissolved and added drop wise to the mixture solution and stirred vigorously for 4 h to form sol. The content of iron was kept constant (0.05 mole %) in all doped samples. The as obtained sol was kept for 24 hr at room temperature to convert into gel. The obtained gel was filtered, washed with methanol and DI water several times and then dried at 100°C for 24 hr. in a hot oven. To obtained fine powder the dried material was ground by mortar and pestle and annealed at 400°C for 4 h to obtain desired co- doped TiO_2 nanoparticles. Similarly, $Ag_xFe_{0.05}Ti_{0.95-x}O_2$; x = 0.08, 0.12 mol % were prepared by using 0.7 and 1.0 gm of $AgNO_3$ in TTIP-methanol solution. The scheme of the synthesis process is presented in Fig. 1.

2.3 Characterization Techniques

The X-ray diffraction measurement was carried out using Cu-Kα radiation of wavelength λ = 1.5406 Å in order to determine the crystalline structure of prepared samples. The optical band gap energy of the silver and iron co-doped TiO_2 nanoparticles was determined from UV–visible absorption spectra recorded at room temperature in the spectral range 200-800 nm. The Photoluminescence spectra were recorded at room temperature in the wavelength region 300-600 nm. The Scanning Electron Microscopic images of silver and iron co-doped TiO_2 nanoparticles were recorded on Scanning Electron Microscope (SEM). The energy dispersive X-ray spectrometer was used to determine the elemental composition present in prepared samples. The Transmission electron microscopic image was recorded on Hitachi (H-7500) microscope. The Fourier Transformation infrared spectra were recorded at room temperature using Perkin Elmer FTIR spectrometer in the spectral range 400-4000 cm^{-1}. The photocatalytic performance of silver and iron co-doped TiO_2 nanoparticles was carried out under visible light source. Separate experiment was conducted for each synthesized sample to observe the photocatalytic activity against degradation of both organic dyes (congo red and methyl orange) in a home-built reactor. 0.05 gm powder of prepared nanoparticles have been dispersed in 100 ml solution of 10^{-5} mol/liter concentration of dyes at room temperature and stirred in dark for 1 hr to achieve equilibrium state. To initiate the degradation process dye dissolved solution was then illuminated by a phosphorus coated mercury vapor lamp using filters

Table 1 — X-ray diffraction measurements parameters of Ag-Fe co-doped TiO_2 nanoparticles

$Ag_xFe_{0.05}Ti_{0.95-x}O_2$	X-ray diffraction angle 2θ (degree)	Crystalline size (nm) calculated from XRD	Crystalline size (nm) calculated from TEM	Optical Band gap energy (Eg) eV
x=0.04 mol %	25.14	48.0	50.5	2.92
x=0.08 mol %	25.14	46.4	--	2.60
x=0.12 mol %	25.14	44.3		2.30

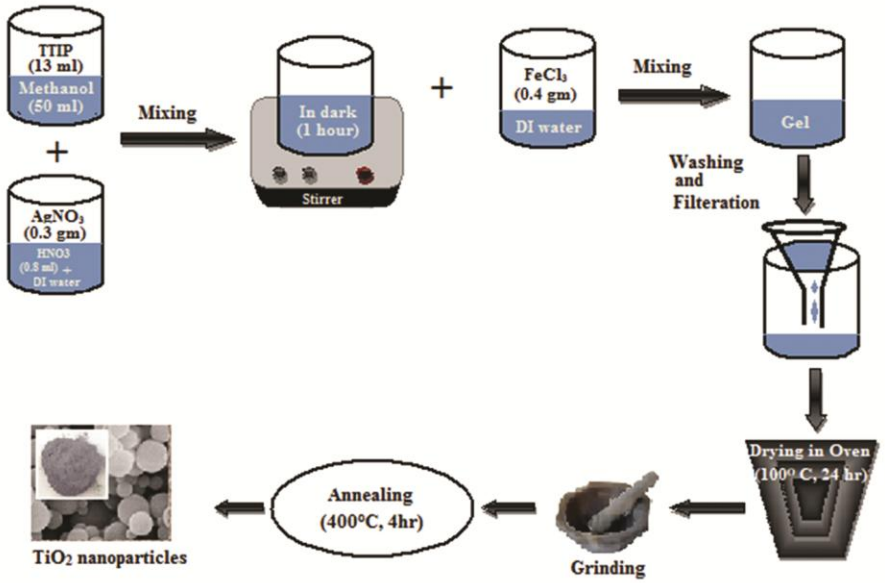

Fig. 1 — Schematic presentation of synthesis process of $Ag_xFe_{0.05}$ $Ti_{0.95-x}O_2$; x = 0.04 mol % synthesized nanoparticles.

of cutoff wavelength from 420 nm to 520 nm. About 3 mL of the dye sample from the reaction beaker was taken out at regular intervals of time 20 min after centrifugation and filtration the photocatalytic activity was observed taking DI water as reference with the help of UV-Vis absorption spectrophotometer.

3 Results and Discussion

3.1 Crystal structural analysis

The recorded X-ray diffraction patterns of prepared samples are displayed in Fig. 2. The XRD analysis of all the samples calcined at 400°C indicate the formation of mixed anatase phase of TiO_2 and Ag_2O. The appearance of characteristic peaks observed at 2θ values 25.41°, 37.94°, 48.11°, 55.19°, 62.86°, 70.53° and 75.26° diffracted from (101), (004), (200), (211), (204), (220) and (215) planes respectively confirm the formation of anatase phase of TiO_2 comparable with JCPDS card no: 84-1285. It has been reported that the doping of silver results in formation of anatase phase and incorporated into TiO_2 lattice not distributed on its surface[25]. However in the present investigation the presence of iron in silver doped TiO_2 nanoparticles is responsible for appearance of

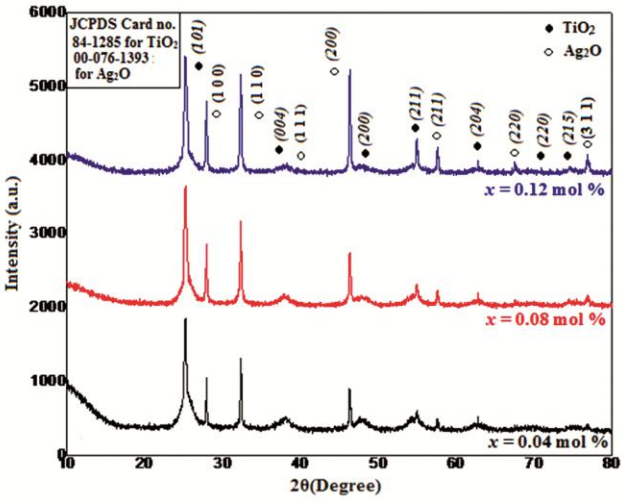

Fig. 2 — X-ray Diffraction pattern of Ag-Fe co-doped TiO_2 nanoparticles.

additional peaks as observed in the XRD spectra at 27.92˚, 32.49˚, 37.94°, 46.35˚, 57.40˚, 67.42˚ and 76.87˚ diffracted from (100), (110), (111), (200), (211), (220) and 311 planes respectively perfectly matched with JCPDS file no.00-076-1393 of Ag_2O phase along with anatase phase of TiO_2, therefore suggest the formation mixed anatase phase of TiO_2

and Ag_2O. However no additional peak corresponds to the presence of iron in the X-ray diffraction pattern indicating the homogeneous distribution of iron species in the TiO_2 matrix. The crystalline size of prepared samples was calculated from FWHM of most dominated (101) peak of anatase phase using Debye-Sherrer's formula[26]

$$D = \frac{k\,\lambda}{\beta cos\theta} \quad \ldots (1)$$

Where k is Scherer's constant (0.9), λ is the wavelength (1.5406 Å) of X-ray radiation, β is full width at half maximum (FWHM) of the most dominated peak and θ is the diffraction angle. The calculated values of crystalline size decreases as the doping concentration increases from 0.04 mole % to 0.12 mole % of silver and are listed in Table 1.

3.2 UV-Visible spectroscopy analysis

The UV-Visible absorption spectra of prepared samples are displayed in Fig. 3(a). The optical band gap was determined using Tauc-Davi and Mott expression[27]

$$(\alpha h\nu)^{1/n} = A(h\nu - Eg) \quad \ldots (2)$$

where α is the absorption coefficient, h is Plank's constant, Eg is the band gap energy, A is the proportionality constant, ν is the frequency of vibrations and n denotes the type of band transition. Here, n = 2 as the absorption of TiO_2 has an indirect transition. The Tauc's plots [plots of $(\alpha h\nu)^{1/2}$ versus photon energy (hν)] of the prepared samples are shown in Fig. 3(b). The linear extrapolation of the curve which cut the energy axis gives the value of the energy band gap (Eg). The determined values of band gap energy are listed in Table 1 and found to decrease with increase in Ag concentration (x).

3.3 Photoluminescence spectroscopy (PL) analysis

The PL spectroscopy is an important technique has been used to estimate the charge carrier trapping, migration, transfer and separation possibility in semiconductor nanoparticles[28]. The recorded PL emission spectra of x=0.04, 0.08 and 0.12 mol% of Ag doped are shown in Fig. 4. The emission peak observed at 390 nm in PL spectra ascribed to the band gap recombination of TiO_2 nanoparticles and is due to annihilation of excitons[29]. The PL peak at 402 nm is shifted to higher wavelength region is due to co-doping of Ag and Fe in TiO_2. It has been reported that

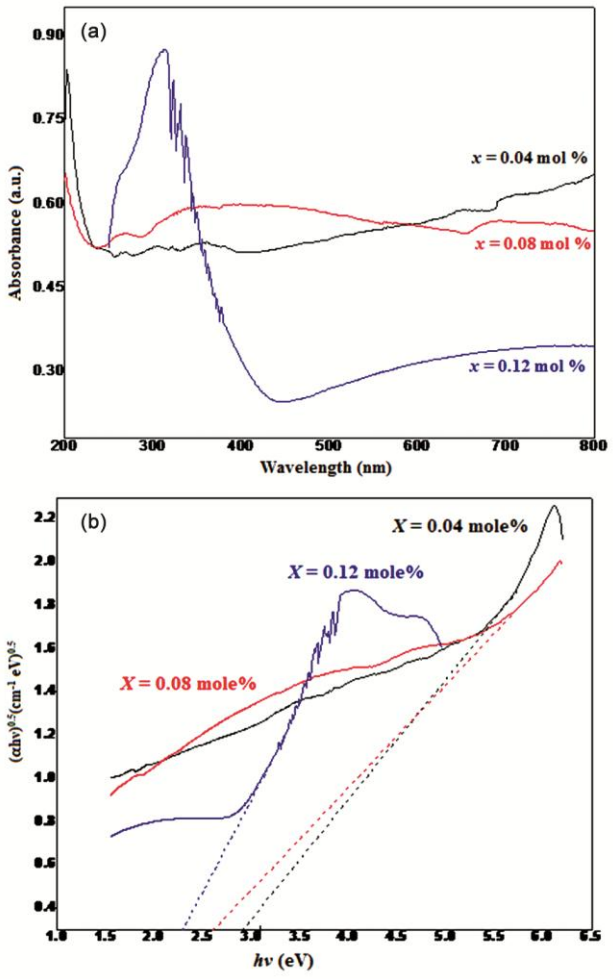

Fig. 3 — (a) UV-Visible absorption spectra of Ag-Fe co-doped TiO_2 nanoparticles, (b) Tauc's Plot of Ag-Fe co-doped TiO_2 nanoparticles.

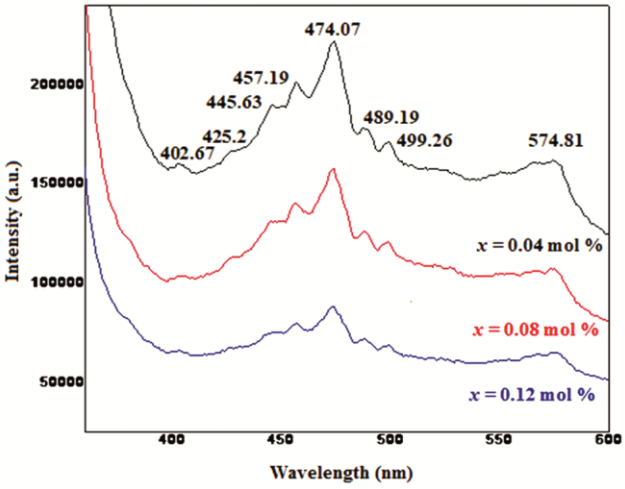

Fig. 4 — Photoluminescence spectra of Ag-Fe co-doped TiO_2 nanoparticles.

the PL peaks observed in the spectral range 300 nm to 600 nm are related to transition from energy states that appears within the forbidden gap to the valance band of TiO_2[30-31]. The emission peaks at 402.67, 445.63, 457.19, 474.07, 489.19, 499.26, 574.81 nm observed in PL spectra indicate the formation of energy states within the forbidden gap of co-doped TiO_2 nanoparticles. It has been reported that the PL emission arises due to the recombination of excited electrons & holes and observed decrease in intensity of PL peaks confirm the decrease in recombination rate of electron–hole pairs[31]. In the present investigation as observed in PL spectra that on increasing Ag content the PL intensity decreases which indicating the high separation efficiency of electron-hole pairs i.e. reduce the charge carrier's recombination rates and enhance the photocatalytic activity. Thus more charge carriers can trap on OH ions to produce reactive OH radicals which are the driving force for photocatalysis process[32].

3.4 Surface Morphological and Elemental composition analysis

The SEM images of synthesized nanoparticles are shown in Fig. 5 (a-c). The SEM images confirm that the nanoparticles are grown in very high density, appear more non-uniform and consist of cluster of particles. The silver (x=0.04 mol %) doped sample shows the formation of somewhat less agglomerated spherical particles with shape and size. On increasing silver concentration (*x*) *i.e. x*= 0.08 mol %, the nanoparticles becomes more agglomerated, irregular in shape, size and finally form the cluster of particles. The SEM image of silver doped sample (*x*=0.12 mol %) shows very big agglomeration. The agglomeration mainly found due to small and mild particles and variable electrical charges present in the atmosphere[2]. It has been reported that the TiO_2 nanoparticles have well defined shape, size and show weak agglomeration and are mainly depends upon synthesis process[33]. Due to formation of cluster of nanoparticles it is very difficult to estimate the actual size of the crystallites. EDX spectroscopy technique is employed to confirm the structural phase formation and chemical composition of the synthesized samples. The EDX analysis clearly showed the presence of Ti, O, Ag and Fe elements as per atomic and weight percentages found in the EDX spectra [Fig. 6 (a-c)] of prepared samples. The titanium and oxygen showing high weight % confirmed that they are the main components in formation of mixed phase of Ag_2O and TiO_2 anatase.

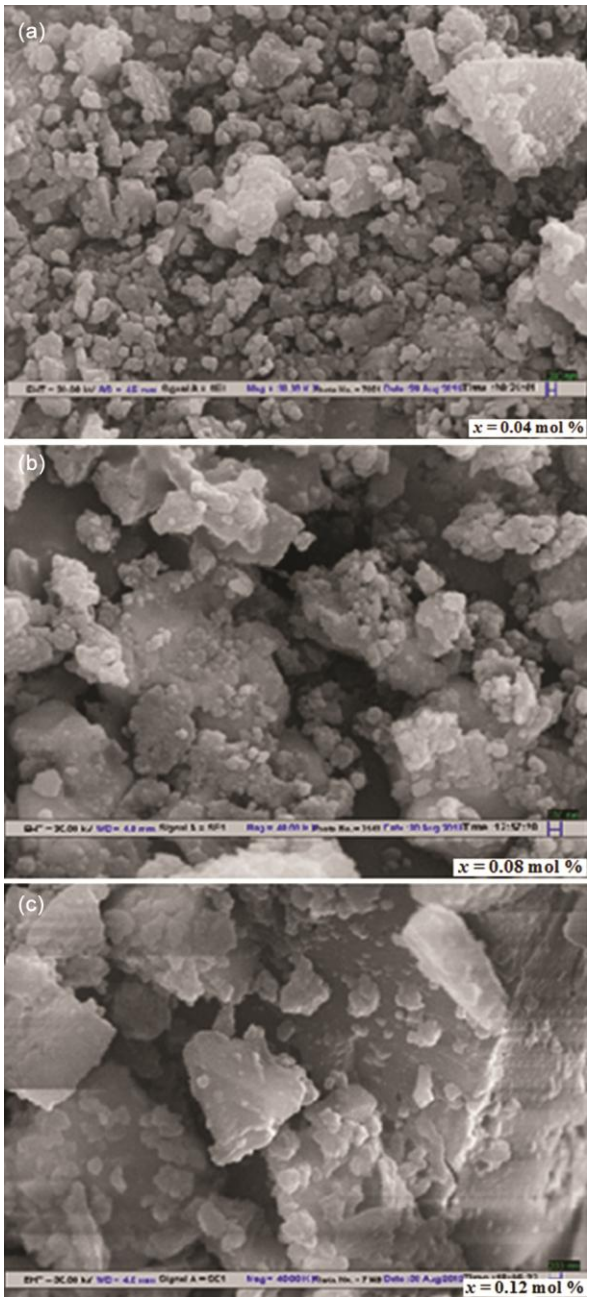

Fig. 5 — (a) FESEM images of Ag-Fe co-doped TiO_2 nanoparticles for *x* = 0.04 mol % of Ag, (b) FESEM images of Ag-Fe co-doped TiO_2 nanoparticles for *x* = 0.08 mol % of Ag, (c) FESEM images of Ag-Fe co-doped TiO_2 nanoparticles for *x* = 0.12 mol % of Ag.

3.5 TEM analysis

To study the growth of formation of the synthesized nanoparticles transmission electron microscopy (TEM) was employed. The TEM micrograph of 0.04 mole % of Ag co- doped nanoparticles is displayed in Fig. 7. Some black dots are observed in TEM micrograph suggests the coexistence of Ag_2O phase as also

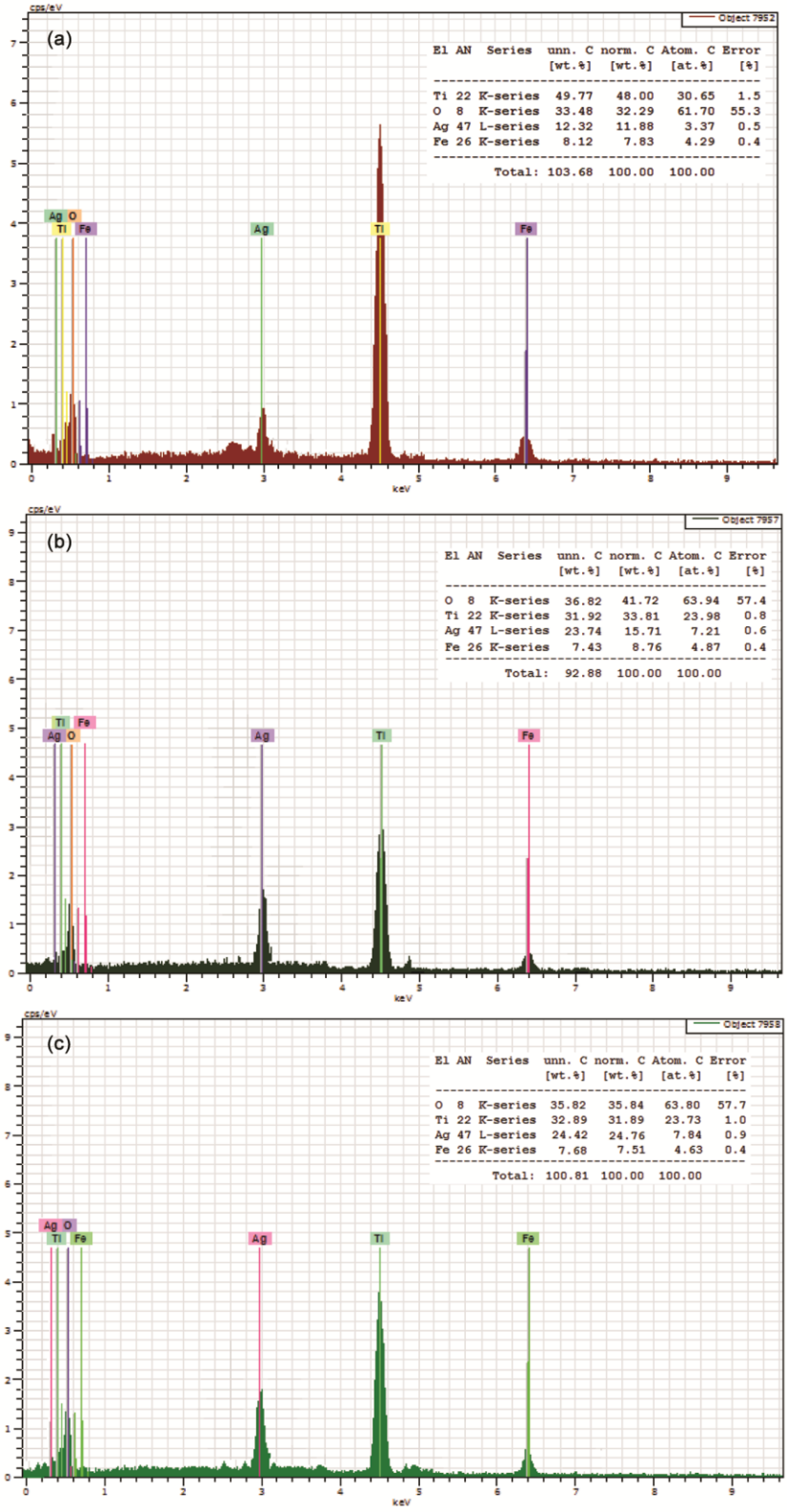

Fig. 6 — (a) EDX spectra of Ag-Fe co-doped TiO_2 nanoparticles for x = 0.04 mol % of Ag, (b) EDX spectra of Ag-Fe co-doped TiO_2 nanoparticles for x = 0.08 mol % of Ag, (c) EDX spectra of Ag-Fe co-doped TiO_2 nanoparticles for x = 0.12 mol % of Ag.

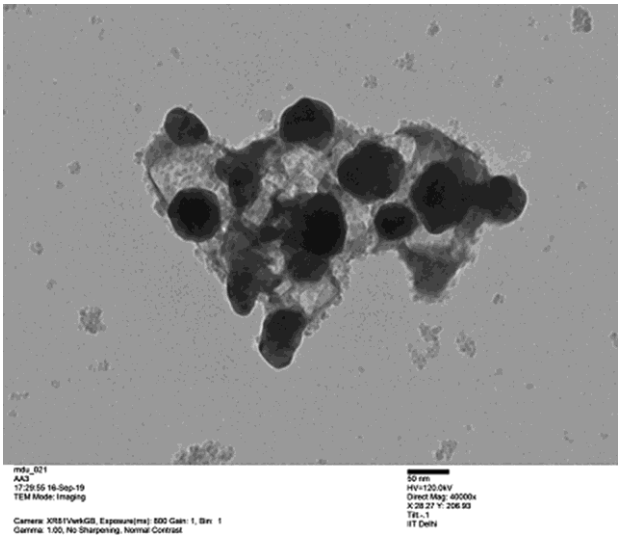

Fig. 7 — TEM image of Ag-Fe co-doped TiO_2 nanoparticles for x = 0.04 mol % of Ag.

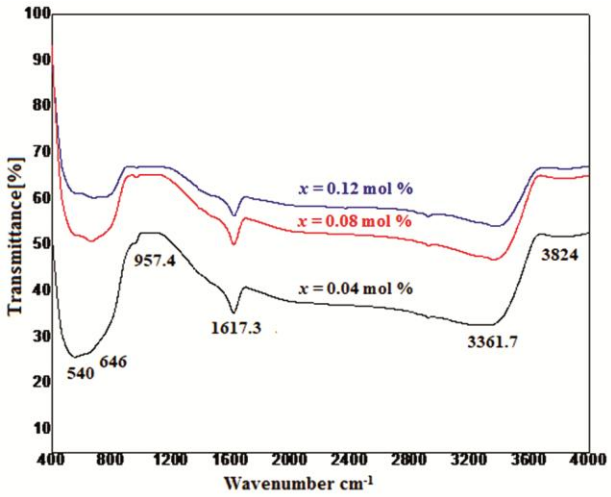

Fig. 8 — FTIR spectra of Ag-Fe co-doped TiO_2 nanoparticles for different mol % of Ag.

observed in XRD data analysis. The appearance of these black dots is due to different crystal structure of Ag_2O and TiO_2.

3.6 FTIR analysis

The main six absorption bands appear at 540, 646, 957.4, 1617.3, 3361.7 and 3824 cm^{-1} and are assigned in the observed FTIR spectra as shown in Fig. 8. It has been reported that absorption bands appeared in the spectral range 450-800 cm^{-1} is assigned to bending vibration of Ti-O-Ti and Fe-O-Fe bending vibrations[34]. In the present spectra bands appear at 540 cm^{-1} and 646 cm^{-1} are assigned to bending vibrations of Fe-O-Fe and Ti-O-Ti stretching bending modes respectively[34-35]. The broad absorption bands

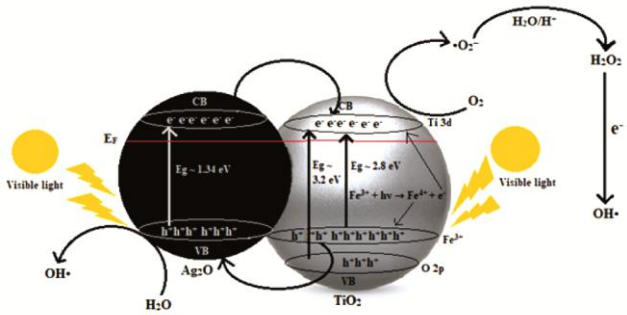

OH• + Dyes → Intermediate products → CO_2 + H_2O

Fig. 9 — Representation of photocatalytic degradation mechanism of silver and iron in Ag-Fe co-doped TiO_2 nanoparticles.

occur at 1617.3, 3361.7 and 3824 cm^{-1} assigned to O-H bending vibrations and are generally occurs due to chemically absorbed water molecules. The formation of hydroxyl and water groups plays key role in generation of photogenerated electron hole pairs which further produce hydroxyl radical (OH) required for degradation of organic dyes[36].

3.7 Photocatalytic degradation activity

The photocatalytic activity of synthesized samples for degradation of organic dyes has been explained on the basis of band diagram (Fig. 9). When the synthesized nanoparticles are exposed to the visible light radiation by absorbing photons of energy equal or higher than their band gap electrons and holes are generated. Electrons (e–) get migrated from lower valence band higher conduction band creating holes (h+) in the valence band. The reaction mechanism goes as follows:

$$TiO_2 + h\nu \text{ (visible)} \rightarrow TiO_2 (e^- \text{ (CB)} + h^+ \text{ (VB)}) \quad \ldots (3)$$

$$Ag_2O + h\nu \text{ (visible)} \rightarrow Ag_2O (e^- \text{ (CB)} + Ag_2O [h^+ \text{ (VB)}] \quad \ldots (4)$$

Generated holes and electrons have tendency of recombination before participation in useful redox reactions but the Ag_2O particles that appears on the surface of TiO_2 can act as electron–hole separation centers[37]. The 3d orbital of Fe^{3+} ion appear above the valence band of TiO_2 absorb photon form light source and produce Fe^{4+} ion and electron these photo-generated electrons get transferred to TiO_2 conduction band[38].

$$Fe^{3+} + h\nu \rightarrow Fe^{4+} + e^- \quad \ldots (5)$$

Due to narrow band gap of Ag_2O (1.34 eV) are sensitive to visible light radiation and due to band

positions of TiO_2 and Ag_2O, the photo generated electrons migrate from Ag_2O conduction band to TiO_2 conduction band and holes from iron 3d state as well as from valance band of TiO_2 to valence band of Ag_2O. This charge transfer process increases the lifetime of the charge carriers and hence reduce the recombination probability and therefore enhance photocatalytic activity[37]. Subsequently, the excited electrons present in conduction band of TiO_2 are actively trapped by O_2 molecules adsorbed at TiO_2 surface to produced superoxide anion ($\bullet O_2^-$) radical and by photonation it yields H_2O_2. This H_2O_2 easily combines with the trapped electrons resulting a photo degradation active species OH• radicals (Eq. 6 - 8).

$$TiO_2\ (e^-\ (CB)) + O_2\ (ads) \rightarrow \bullet O_2^- \quad \ldots (6)$$

$$2\bullet O_2^- + 2H^+ \rightarrow 2HO_2^{\bullet} \rightarrow H_2O_2 + O_2 \quad \ldots (7)$$

$$H_2O_2 + TiO_2\ (e^-\ (CB)) \rightarrow OH\bullet + OH^- \quad \ldots (8)$$

In addition, the photogenerated holes in Ag_2O valence band directly react with surface adsorbed water molecules to produce OH• radicals. Due to oxidation and reduction process the intermediate dye product further completely mineralized the formation of carbon dioxide and water[39]. The detailed reactions are described by Equations (9-10) as follows:

$$(H_2O \leftrightarrow H^+ + OH^-)\ ads + h^+\ (VB) \rightarrow OH\bullet + H^+ \quad \ldots (9)$$

$$Dye + OH\bullet \rightarrow Intermediate\ products \rightarrow CO_2 + H_2O \quad \ldots (10)$$

It is observed that under visible light source holes are accumulate on the surface of Ag_2O and electrons to the TiO_2 surface as a result TiO_2 becomes anionic and Ag_2O becomes cationic in nature. Moreover, Ag_2O is appears on the TiO_2 surface and behaves as cationic nature. As methyl orange and congo red dyes are anionic in nature therefore in an aqueous solution the anionic dye radicals experience columbic attraction with cationic Photocatalyst surface and get adsorbed[37]. The relationship between concentration and time, behavior of Photocatalyst during reaction can be determined using first-order reaction[40]

$$log\left(\frac{C}{Co}\right) = kt \quad \ldots (11)$$

Where co and c are the initial concentration of dye at time t = 0 and concentration of dissolved dye at time t respectively. k represents apparent rate constant. The graph [Fig. 10 (a-b)] is plotted between

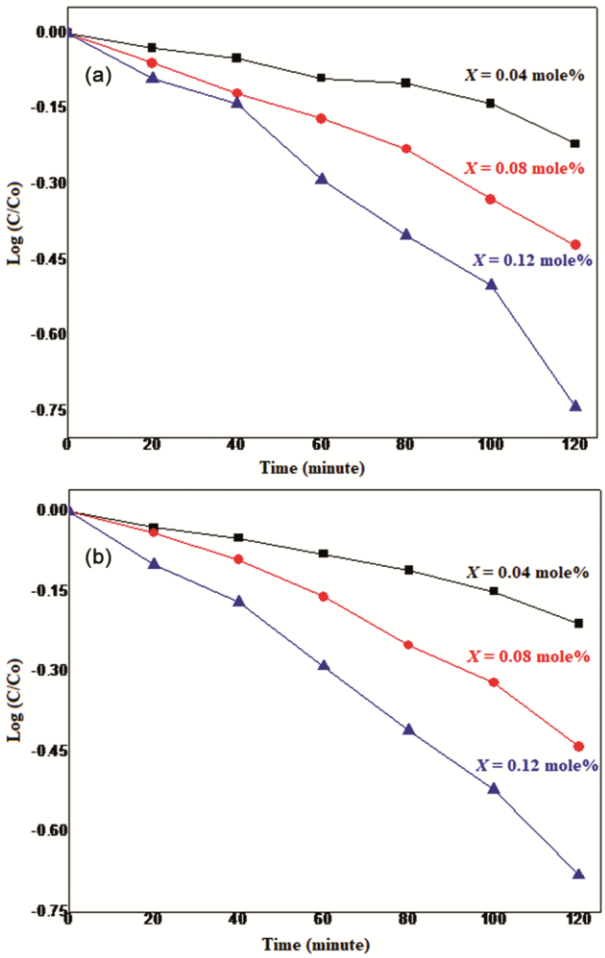

Fig. 10 — (a) The graph between log (c/co) vs time for congo red dye at 120 minutes, (b) The graph between log (c/co) vs time for methyl orange dye at 120 minutes.

log (c/c_o) and time for both dyes and show linear behavior. The observed average value of rate constant k (at 120 min.) for congo red and methyl orange are 3.8×10^{-3} min^{-1} and 3.6×10^{-3} min^{-1} respectively determined from the slope of the graph [Fig. 10 (a-b)] During photocatalytic process the photo generated electron-hole pairs and increase in surface charge on TiO_2 in synthesized nanoparticles helps in degradation of organic dyes. The regular decrease in log (c/c_o) with time clearly indicates the decrease in concentration of both dissolved dyes. Degradation of dye in dark was found to be negligible. The photocatalytic efficiency was calculated by using following equation

$$\eta\ (\%) = \frac{co - c}{co} \times 100 \quad \ldots (12)$$

Here co and c are the initial concentration of dye at time t = 0 and concentration of dissolved dye at time t

Table 2 — Percentage degradation of methyl orange & Congo red dyes after exposure to visible light source of Ag-Fe co-doped TiO_2 nanoparticles.

Exposure time (Minutes)	Congo Red			Methyl Orange		
	$x = 0.04$	$x = 0.08$	$x = 0.12$	$x = 0.04$	$x = 0.08$	$x = 0.12$
0	0	0	0	0	0	0
20	6	13	19	6	8	21
40	11	24	28	11	19	33
60	18	33	49	17	31	49
80	21	41	60	23	44	61
100	27	53	71	29	52	70
120	39	62	82	38	64	79

respectively It is observed that the concentration of dyes decreases with increasing exposure time and synthesized nanoparticles degraded both the dyes to larger extent with increasing Ag content. The experimental determined values of percentage degradation of organic dyes are tabulated in Table 2. These results suggest that increase in doping concentration enhance the photocatalytic activity of synthesized nanoparticles.

Conclusion

In the present report the Ag and Fe co-doped TiO_2 nanoparticles were synthesized by sol-gel technique on varying the concentration of Ag (x = 0.04, 0.08 & 0.12 mol %) by keeping the fixed concentration of iron. The prepared nanoparticles exhibits mixed anatase phase of TiO_2 with Ag_2O as evaluated from X-ray diffraction measurements and further verified from the elemental compositions of the constituent's presents in the samples determined from EDX measurements. The crystalline size and band gap energy were found to decrease with further increase in doping concentration (x). The appearance of emission bands in PL spectra confirms the existence of energy sub states with the forbidden gap TiO_2 nanoparticles. The surface morphology was estimated from FESEM micrographs which indicate the formation of clusters of nanoparticles. The appearance of black dots in TEM micrograph confirms that the doping of Ag is not completely incorporated and appears on the surface of TiO_2. The formation of different functional groups as observed in FTIR spectra plays key role to accelerate photocatalytic activity. Further increase in Ag doping concentration enhances the photocatalytic activity for degradation of organic dyes.

References

1 Naraginti S, Thejaswini T V L, Prabhakaran D, Sivakumar A, Satyanarayana V S V & Prasad A, *Mol Biomol Spectrosc*, 149 (2015) 571.

2 Avciata O, Benli Y, Gorduk S & Koyun O, *J Eng Technol Appl Sci*, 1 (2016) 34.

3 Kundu V S, Chauhan N & Kumar S, *Indian J Pure Appl Phys*, 55 (2017) 881.

4 Pirzada B M, Mehraj O, Ahmad B S & Sabir S, *J Environ Chem Eng*, 6 (2018) 3204.

5 Hassan A, Asad M, Jechan L, Ki- Hyun K, Jae-Woo P & Alex C K Y, *Nano Res*, 22 (2019) 995.

6 Ajmal A, Majeed I, Malik R N, Idriss H & Nadeem M A, *RSC Adv*, 4 (2014) 37003.

7 Mohammed I, *J Environ Chem Eng*, 8 (2020) 103676.

8 Ebrahimi R, Maleki A, Rezaee R, Daraei H, Safari M, Mckay G, Mok-Lee S & Jafari A, *Arab J Sci Eng*, 46 (2021) 6409.

9 Chen D, Cheng Y, Zhou N, Chen P, Wang Y, Li K, Huo S, Cheng P, Peng P, Zang R, Wang L, Liu Y & Ruan R, *J Clean Product*, 268 (2020) 121725.

10 Seery M K, George R, Floris P & Pillai S C, *J Photochem Photobiol A: Chem*, 189 (2007) 258.

11 Bagheri S, Ramimoghadam D, Yousefi A T & Abd H S B, *Int J Electrochem Sci*, 10 (2015) 3088.

12 Ambrus Z, Balazs N, Alapi T, Wittmann G, Sipos P, Dombi A & Mogyorosi K, *Appl Catal B: Environ*, 81 (2008) 27.

13 Kumar S, Singh A P, Yadav N, Thirumal M, Mehta B R & Ganguli A K, *Chem Select*, 1 (2016) 4891.

14 Chen X & Mao S S, *Chem Rev*, 107 (2007) 2891.

15 Mogal S I, Gandhi V G, Mishra M, Tripathi S, Shripathi T, Joshi P A & Shah D O, *Ind Eng Chem Res*, 53 (2014) 5749.

16 Mohamed A I, Mohamed N H, Dalaver H A, Venkatesh S & Suk H C, *Catalyst*, 11 (2021) 438.

17 Siripond P, Tuksadon W, Panita K, Suchinda S, Tippabust E & Chaweewan S, *Mater Res Bullet*, 148 (2022) 111668.

18 Antonietta M, Olga S, Vincenzovaian, Diana S, Stefania P, Vincenzo V & Nicola M, *Catal Today*, 380 (2021) 93.

19 Nguyen T T M, Nguyen K N, Dang T M H, Ta N D, Huynh D C & Tran Q H, *Adsorpt Sci Technol*, 2021 (2021) 9193052.

20 Rani A, Dhiman R L, Singh V, Kumar S & Kumar S, *Nano Express*, 2 (2021) 030002.

21 Charitha T & Shanitha M, *J Sol-Gel Sci Technol*, 99 (2021) 109.

22 Basavarajappa P S, Patil S B, Ganganappa Na, Reddy K R, Raghu A V & Reddy C V, *Mater Sci Int J Hydrogen*, 45 13 (2020) 7764.

23 Paul A C, Chao C, Koosha A, Bernd G, Mumin M A, Lotus A F, Therrien P & Mittler S, *Nanotechnology*, 30 (2019) 85706.

24 Charitha T & Shanitha M, *J Sol-Gel Sci Technol*, 99 (2021) 109.

25 Chen C, X F Lei & Xue M Z, *J Chem Res*, 41 (2017) 475.
26 Cullity B D, *Elements of X-ray Diffraction, Reading Mass: Addison–Wesley Publishing Co*, (1956) 352.
27 Davis E A & Mott N F, *Philos Mag*, 22 (1970) 903.
28 Lettieri S, Pavone M, Fioravanti A, Amato L S & Maddalena P, *Materials*, 14 (2021) 1645.
29 Komaraiah D, Radha E, Kumar J S, Reddy M V R & Sayanna R, *Opt Mater*, 108 (2020) 110401.
30 Pugazhenthiran N, Murugesan S & Anandan S, *J Hazard Mater*, 263 (2013) 541.
31 Liang D Y, Cui C, Hu H H, Wang Y P, Xu S, Ying B L, Li P G, Lu B Q & Shen H L, *J Alloys Compd*, 582 (2013) 236.
32 Ocwelwang A R & Tichagwa L**,** *Int J Adv Res Chem Sci*, 1 (2014) 28.
33 Praveen P, Viruthagiri G, Mugundan S & Shanmugam N, *Spectrochim Acta Part A: Mol Biomol Spectrosc*, 117 (2014) 622.
34 Buzuayehu A, Murthy H C A & Dessie Y, *Arab J Sci Eng*, 45 (2020) 4609.
35 Yang G D, Jiang Z, Shi H H, Xiao T & Yan Z F, *J Mater Chem***,** 20 (2010) 5301.
36 Ali T, Ahmed A, Alam U, Uddin I, Tripathi P & Munner M, *Mater Chem Phys*, 212 (2018) 325.
37 Paul K K, Ghosh R & Giri P K, *Nanotechnology*, 27 (2016) 315703.
38 Ali T, Tripathi P, Ameer A, Waseem R, Ahmed A S, Ahmed A & Muneer M, *Mater Chem Phys*, 212 (2018) 325.
39 Sirivallop A, Areerob T & Chiarakorn S, *Catalyst*, 10 (2020) 251.
40 Tolosa N C, Lu M C, Mndoza H D & Rollon A P, *Appl Catal A Gen*, 401 (2011) 233.